We are IntechOpen, the world's leading publisher of Open Access books Built by scientists, for scientists

5,000
Open access books available

125,000
International authors and editors

140M
Downloads

Our authors are among the

154
Countries delivered to

TOP 1%
most cited scientists

12.2%
Contributors from top 500 universities

CLARIVATE ANALYTICS
BOOK CITATION INDEX
INDEXED

WEB OF SCIENCE™

Selection of our books indexed in the Book Citation Index
in Web of Science™ Core Collection (BKCI)

Interested in publishing with us?
Contact book.department@intechopen.com

Numbers displayed above are based on latest data collected.
For more information visit www.intechopen.com

Heat Transfer and Fluid Flow Investigations in PDMS Microchannel Heat Sinks Fabricated by Means of a Low-Cost 3D Printer

Inês Maia, Cesar Rocha, Pedro Pontes, Vanessa Cardoso, João M. Miranda, Ana S. Moita, G. Minas, António L.N. Moreira and Rui Lima

Abstract

Polydimethylsiloxane (PDMS), due to its remarkable properties such as optical transparency and ability to easily mold, is one of the most popular polymers used in micro- and nanofluidics. Furthermore, 3D printing technology due to its low cost and simplicity is also gaining a great interest among the microfluidic community. In this work, the potential of 3D printing is shown to produce microfluidic devices, their ability for studying flows and heat transfer of nanofluids, and their applicability as a heat sink device. The low-cost fused deposition modeling 3D printing technique was combined with a PDMS casting technique for the microfluidic device fabrication. The potential of this technique was experimentally demonstrated by fluid flow and heat transfer investigations using different fluids, such as distilled water-, alumina (Al_2O_3)-, and iron oxide (Fe_3O_4)-based nanofluids. The simplicity, low-cost, and unique features of the proposed heat sink device may provide a promising way to investigate nanofluids' flow and heat transfer phenomena that are not possible to be studied by the current traditional systems.

Keywords: microfluidics, 3D printing, microchannel heat sinks, nanofluids, heat transfer, electronics cooling

1. Introduction

The continuous investigation on strategies for size reduction while maintaining, or even increasing, power of technological devices demands cooling systems with higher thermal efficiency and smaller sizes. One approach relied on the modification of heat sinks by incorporating microchannels to increase the heat exchange surface. Despite being a well-adopted strategy, its complex configurations proved to be difficult to manufacture [1, 2]. Other strategies focused on the type of the used fluids for the cooling process. Dielectric fluids [1, 3], two-phase fluids [3, 4], and nanofluids (NFs) [5–8] have been thoroughly investigated. Among these three,

the nanofluids, which are fluids comprised of particles, with size ranging from 1 to 100 nm, suspended in a base fluid, have been reported as presenting a better thermal conductivity than the base fluid [8, 9]. Nevertheless, some challenges regarding their usage, such as agglomeration, long-term stability, and high-costs, still need further investigation [8, 10–12]. The most commonly used nanoparticles (NPs) for NFs are metallic, such as Cu, Ag, Au, and Fe, or non-metallic such as Al_2O_3, CuO, TiO_2 SiC, and carbon nanotubes. Many authors reported that the heat transfer of NFs is influenced by several factors such as shape, dimensions, volume fractions in the suspensions, and the thermal properties of the particle materials [11, 13, 14]. Therefore, enhancement in heat transfer was also reported, but only for small concentrations of NPs [8, 9].

Abareshi et al. [15] have evaluated the thermal conductivity of nanofluids with different volume fractions of Fe_3O_4 NPs, at different temperatures. The thermal conductivity was reported to increase up to 11.5% for a volume fraction of 3 vol% at 40°C. Xia et al. [16] have investigated the heat transfer coefficient of nanofluids using TiO_2 and Al_2O_3 NPs, with different volume fractions. For a volume fraction of 1%, the heat transfer coefficient was significantly increased for both nanofluids, compared with deionized water. Gavili et al. [17] have studied the thermal conductivity of ferrofluids with Fe_3O_4 particles of approximately 10 nm in diameter, suspended in deionized water. With the application of a magnetic field, the thermal conductivity was increased up to 200% for a 5% volume fraction. Kim et al. [18] have investigated the thermal conductivity of alumina- and distilled water-based nanofluids, with concentrations of 0.5, 1, and 2 wt%. The conductivity was found to increase with the increasing of the NPs concentration. Al-Rjoub et al. [19] have tested four cooling liquids: deionized water; distilled water; borax buffer; and Al_2O_3 NPs solution, on a microscale heat exchanger. It was found that the deionized water has presented the lowest heat removal capacity, while the Al_2O_3 solution showed the highest capacity, corresponding to about 69% increase.

The majority of microchannel heat sink devices that can be found in literature were fabricated in silicon, due to its thermal conductivity. However, the fabrication process of those devices can be laborious and needs extremely expensive facilities. Novel, fast, and low-cost fabrication techniques have been developed by means of different kinds of polymers [20–22]. PDMS is a silicone elastomer with a set of properties that make it suitable for many applications and is a popular choice for microfluidic devices fabrication [21, 22]. Besides being cheaper than the monocrystalline silicon, it presents a low elasticity change versus temperature, high thermal stability, chemical inertness, dielectric stability, shear stability, high compressibility, and hyperelasticity [23–27]. Moreover, it is non-toxic and biocompatible [25, 27–29]. PDMS devices can be manufactured by simple techniques at room temperature, such as replica molding.

The 3D printers are gaining an increased attention by both academic and industrial community to produce microdevices and models at an extremely low cost. Some successful applications can already be found in lab-on-a-chip tools [30], microfluidics [31, 32], and biomedical *in vitro* devices [27, 32–34]. There are different kinds of printing methods such as the Fused Deposition Modeling (FDM) and stereolithography [32]. Among those methods, the most popular, simple method with the lowest cost is the FDM technology [32]. For this reason, the FDM process was combined with a PDMS casting technique to produce a PDMS microfluidic device. Hence, the main objective of this work is to show the potential of a FDM 3D printer to produce microfluidic devices and their potential to be used to perform flows and heat transfer studies of nanofluids. To demonstrate the potential of this technique, fluid flow and heat transfer studies were performed by using different fluids such as distilled water-, alumina (Al_2O_3)-, and iron oxide (Fe_3O_4)-based nanofluids with concentrations of 1 and 2.5%.

2. Materials and methods

This section describes the experimental protocol to develop the nanofluids and the fabrication process to produce the heat sinks, as well as the used experimental setup.

2.1 Nanoparticles preparation

Two different types of NPs were used on the flow and heat experiments: alumina oxide (Al_2O_3) NPs acquired from Sigma Aldrich (ref. 702,129, Sigma Aldrich) and iron oxide (Fe_3O_4) NPs synthesized on our laboratory by co-precipitation. This last method allows to produce magnetic iron oxide NPs in a cost-effective way and is appropriate for mass production. The Al_2O_3 NPs had a size inferior to 50 nm, while the synthesized Fe_3O_4 NPs had an average size of 11 ± 2 nm.

The co-precipitation was initiated with the preparation of the precipitation agent by adding 0.01 g of cetrimonium bromide (CTAB), diluted in 3 mL of distilled water, to 20 mL of ammonium hydroxide (NH_4OH). Hereinafter, a ferrous solution was prepared by diluting 7.78 g of iron(III) chloride ($FeCl_3$) and 4.06 g of iron(II) chloride ($FeCl_2$) in 20 mL of distilled water, in an ultrasonic bath. The solution was subsequently mechanically stirred at, approximately, 1500 rpm. The precipitation solution was then added, dropwise, to the ferrous solution under stirring, on a laminar flow cabinet. The co-precipitation occurred according to the following equation:

$$FeCl_2.4H_2O_{(l)} + 2FeCl_3.6H_2O_{(l)} + 8NH_4(OH)_{(aq)}$$
$$= Fe_3O_{4(s)} + 8NH_4Cl_{(aq)} + 20H_2O_{(l)} \qquad (1)$$
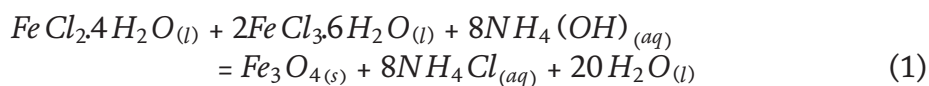
To conclude the process, the NPs were washed several times with distilled water with the assistance of a strong magnet.

Figure 1 shows the synthesized NPs and the representative transmission electron microscopy (TEM) image. A detailed description of this process can be found at Cardoso et al. [35].

Despite the TEM images show the aggregates of Fe_3O_4 NPs, in the NF, they were stable and non-aggregated for a period of time after 10 min of ultrasonic bath.

The NPs show a normalized magnetization of ~69 emu.g 1 at ~10 kOe, which corresponds to the saturation magnetization, and also show a superparamagnetic behavior with an extremely low coercivity of 1.6 Oe [35–37].
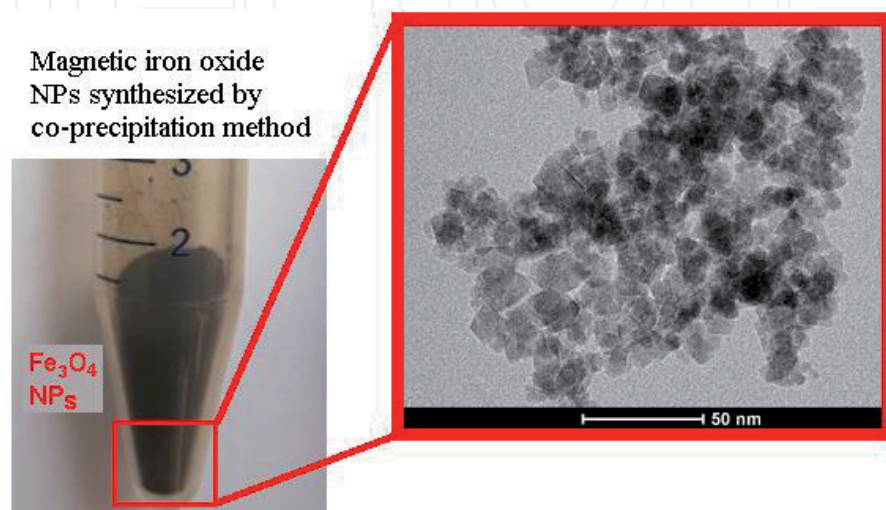

Figure 1.
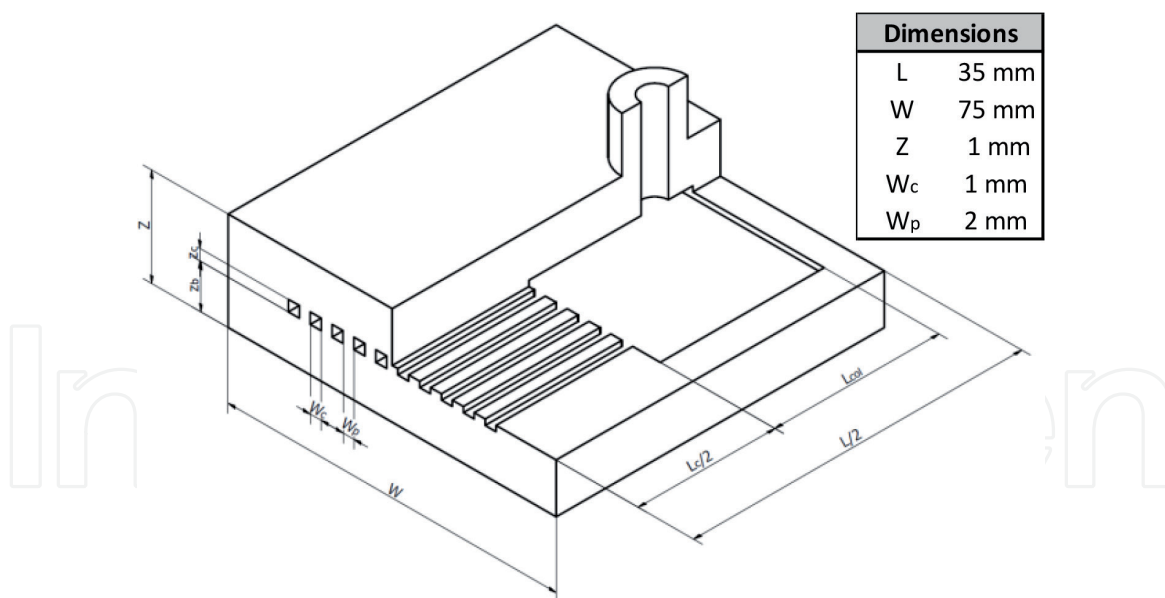*Magnetic iron oxide NPs and representative TEM image, adapted from [35, 36].*

Dimensions	
L	35 mm
W	75 mm
Z	1 mm
Wc	1 mm
Wp	2 mm

Figure 2.
Schematic representation of the main dimensions of the ABS master mold.

2.2 Fabrication of the heat sink microchannel

The heat sink microchannel device was produced based on a scaffold-removal technique [25]. First, the molds were drawn by using the Autodesk Inventor® software and then printed at the FDM 3D printer Ultimaker 2+ (Ultimaker, Netherlands). The first mold was printed with acrylonitrile butadiene styrene (ABS), whereas the second one was printed with polylactic acid (PLA). The fabrication of the molds was performed with a nozzle with a diameter of 0.4 mm, whereas the layer resolution was about 100 μm. The main dimensions of the ABS master mold can be found in **Figure 2**.

Once the 3D models were printed, PDMS was prepared by adding a PDMS curing agent into the pre-polymer with a mixing ratio of 1:10. The PDMS was poured onto the PLA mold with the ABS master mold inside it. Once the PLA mold was filled with PDMS, the elastomer was cured at room temperature for about 1 day. Finally, the PDMS was removed from the PLA mold and immersed in an acetone bath to remove the ABS for approximately 24 h. **Figure 3** shows the schematic diagram of all the main steps to produce the PDMS heat sink device. The overall cost to fabricate the PDMS heat sink device is about 3.8 €. This cost includes the printing of the ABS master mold (~1 €) and PDMS casting process (~2.8 €).

Notice that after the PDMS curing process, small holes were made below the inlet and outlet to insert the thermocouples (type K). **Figure 4** shows the PDMS heat sink microfluidic device used in the flow and heat experiments.

2.3 Experimental procedures

The PDMS heat sink was placed on top of a hot plate controlled by a 9400-temperature controller (CAL Controls). The temperature of the plate was set to 60°C, whereas the flow rate of the fluids was controlled by a syringe pump (Harvard) connected to the inlet of the heat sink. The temperature at the entrance and exit of the device was acquired through a data acquisition instrument connected to the thermocouples of the device. Wood and polystyrene blocks were used to minimize the heat losses. **Figure 5** shows a schematic diagram of the experimental setup. The flow of the Fe_3O_4 nanofluid was analyzed by optical microscopy at a flow rate of 10 μL/min. Note that the temperature measurements presented
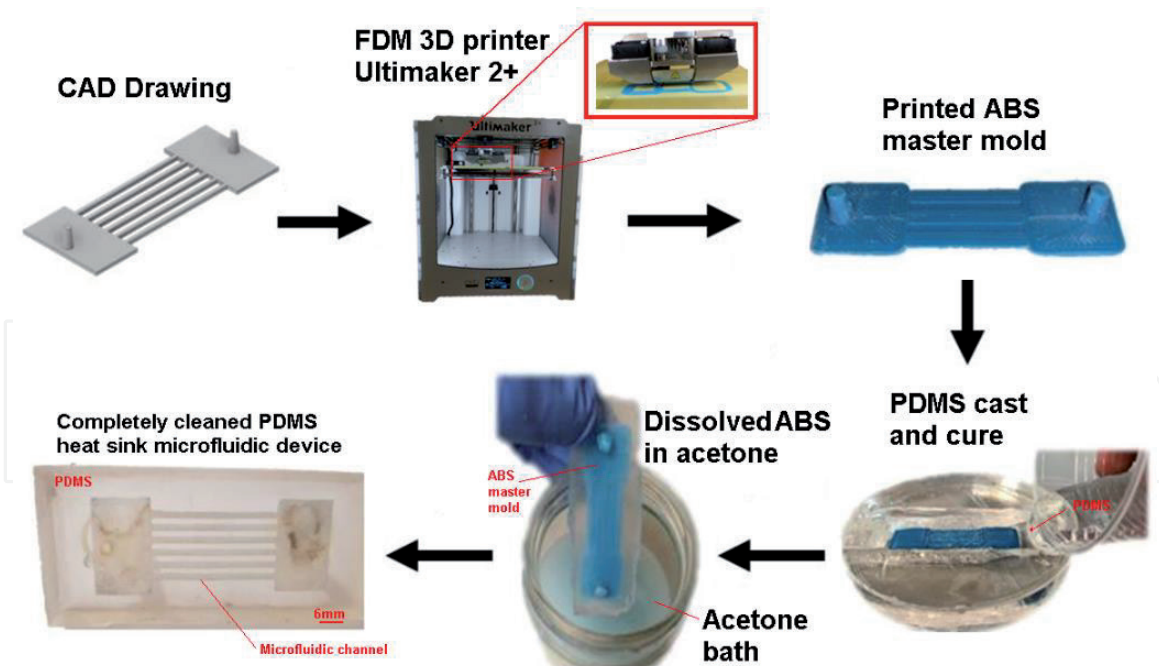
Figure 3.
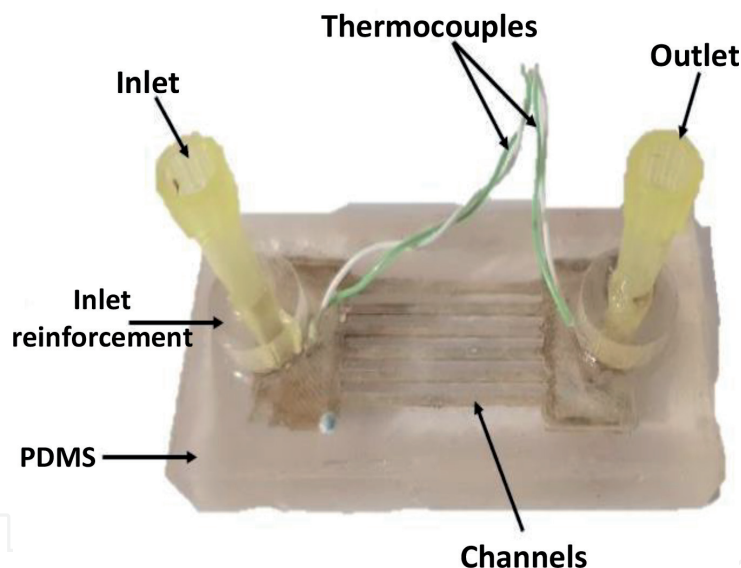*Schematic representation of main steps to fabricate the PDMS heat sink.*

Figure 4.
PDMS heat sink microfluidic device with the inserted thermocouples.

an uncertainty of ±1°C. The thermographic studies were performed with distilled water at a flow rate of 1, 5, 7.5, 10, and 15 mL/min and a thermographic camera Onca-MWIR-InSb (Xenics Infrared Solutions). The setup and calibration procedures of the camera were performed as in Teodori et al. [38]. Images, with a resolution of 150px × 150px, were taken with a frame rate of 1000 fps.

To evaluate the influence of the nanofluids properties in the heat sink microfluid device, the tests were performed using distilled water, Fe_3O_4 at a concentration of 1 and 2.5%, and Al_2O_3 at the same concentrations. All the fluids were set to a flow rate of 1 up to 30 mL/min.

2.4 Heat transfer calculations

The properties of the nanofluids were obtained taken into account fundamental equations described on previous studies [39, 40]. The thermal conductivity of the
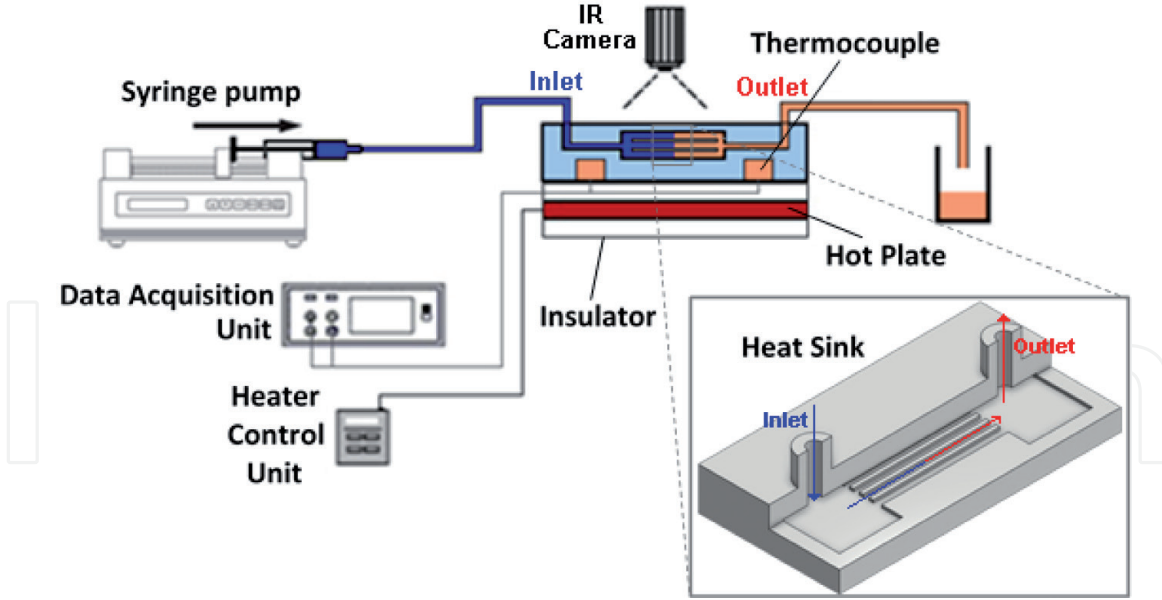
Figure 5.
Schematic representation of the experimental setup.

nanofluid was obtained according to the Maxwell model described by the following Equation [39, 40]:

$$K_{nf} = K_{bf}\left(\frac{K_p + 2K_{bf} + 2\varphi(K_p - K_{bf})}{K_p + 2K_{bf} - 2\varphi(K_p - K_{bf})}\right), \tag{2}$$

where K_{nf} is the nanofluid thermal conductivity, K_p is the NPs thermal conductivity, K_{bf} is the base fluid thermal conductivity, and φ is the NPs concentration.

The nanofluid density and heat capacity were calculated through the weighted average of the individual properties of both the NPs and base fluid. The first is expressed by Eq. (3) [14, 41] and the latter by Eq. (4) [11, 14].

$$\rho_{nf} = \rho_p \varphi + \rho_{bf}(1 - \varphi), \tag{3}$$

$$c_{p_{nf}} = \varphi \rho_p c_{p_{np}} + (1 - \varphi) \rho_{fb} c_{p_{bf}} \tag{4}$$

In the abovementioned equations, ρ_{nf} represents the nanofluid density, ρ_p the particle density, ρ_{bf} the base fluid density, and $c_{p_{np}}$ and $c_{p_{bf}}$ the specific heat capacity of the NPs and of the base fluid, respectively.

The nanofluid viscosity was determined through the equation proposed by Batchelor [42]:

$$\mu_{nf} = \left(1 + 2.5\varphi + 6.2\,\varphi^2\right)\mu_{fb}, \qquad 0 < \varphi < 10\% \tag{5}$$

where μ_{nf} is the nanofluid viscosity and μ_{fb} the base fluid viscosity. This equation brings in a quadratic dependence with the volume fraction, which provides a better representation of the interaction between the particles on the fluid.

Within the microfluidic device, the heat transfer will occur by convection inside the microchannels and by conduction in the walls between them. Consequently, the mathematical approach that better allowed the evaluation of the heat transfer was described by Ma et al. [10]. The convection heat transfer coefficient was calculated by iterations using the following equations:

$$h = \frac{Q}{N(A_b + 2\eta A_l)(T_b - T_{avgf})}, \tag{5}$$

$$m_i = \sqrt{\frac{2h_{i-1}}{k_{PDMS}.w_p}}, \tag{6}$$

$$\eta_i = \frac{th\,(m_i z_c)}{m_i z_c}, \tag{7}$$

where A_b represents the area of microchannel bottom, A_l the area of microchannel sidewall, T_{avgf} the average temperature of the fluid, η the fin efficiency, w_p the average width of fin, and z_c the height of the channel. The main dimensions of the heat sink are illustrated in **Figure 2**. The heat transfer rate, Q, represents the amount of heat energy taken by the fluid when it flows through the channels and is given by Eq. (9). This parameter was obtained for each mass flow rate, $\dot{m}$, after the temperature at the inlet, T_{in}, and at the outlet, T_{out}, were measured.

$$Q = q\,\rho_f c_{pf}(T_{out} - T_{in}), \tag{8}$$

where q, c_{pf}, and ρ_f is the volume flow rate, specific heat capacity, and density of the working fluid, respectively.

3. Results and discussion

In this section, the obtained results are presented and discussed. The temperature measurements and the known properties of the materials were used to calculate the parameters described on the previous section. Using those parameters, the influence of the environment conditions and of the fluid properties in heat transfer was analyzed.

3.1 Influence of the nanofluid properties

As described previously, the prepared nanofluids with iron oxide (Fe_3O_4) and alumina (Al_2O_3) NPs were used to verify the thermal properties influence of the nanofluids in the heat transfer performance of the developed PDMS heat sink device.

Figure 6 shows the temperature difference between the inlet and the outlet as the tested nanofluids flow through the proposed PDMS heat sink. Overall, it is possible to conclude that both tested nanofluids present a bigger temperature difference between the inlet and the outlet in comparison with distilled water. Hence, these measurements indicate that the amount of heat energy absorbed by both nanofluids was bigger than that absorbed by the distilled water. In addition, the amount of heat absorbed by the nanofluids was found to be bigger for smaller flow rates, as shown in **Figure 6**. These results corroborate the measurements performed by Chein and Chuang [43], where they have investigated the heat performance of nanofluids with CuO NPs in a microchannel heat sink. These results also show that the flow rate affects the amount of heat absorbed by the nanofluids.

In **Figure 7**, an increase of the convective heat transfer coefficient was registered on both nanofluids, in comparison to the base fluid. The increase was more pronounced for the alumina nanofluid due to the greater stability of the nanofluid and bigger thermal conductivity of these kind of NPs [6]. By increasing the convective heat transfer coefficient, an increase of the heat transfer rate is expected. In **Figure 8**, it is possible to observe an increase in the heat transfer rate for both tested nanofluids in comparison with distilled water. From these results, it is also possible to conclude that for both nanofluids, the convective heat transfer coefficient and heat transfer rate increase with the flow rate, which agrees with the results obtained by Wen and Ding [44].
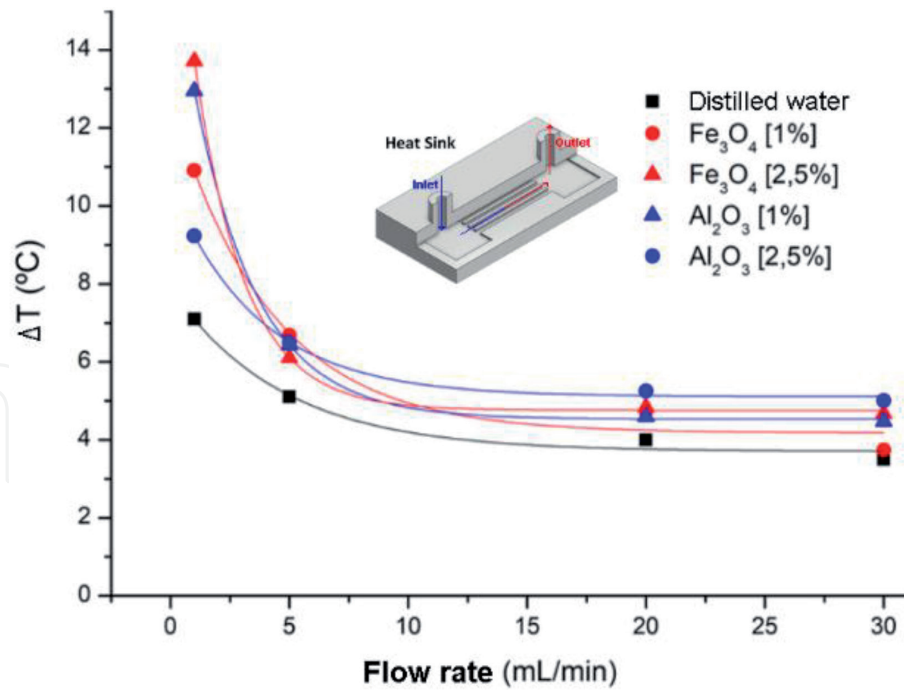
Figure 6.
Temperature difference between the inlet and the outlet for the tested nanofluids at the proposed PDMS heat sink microfluidic device.
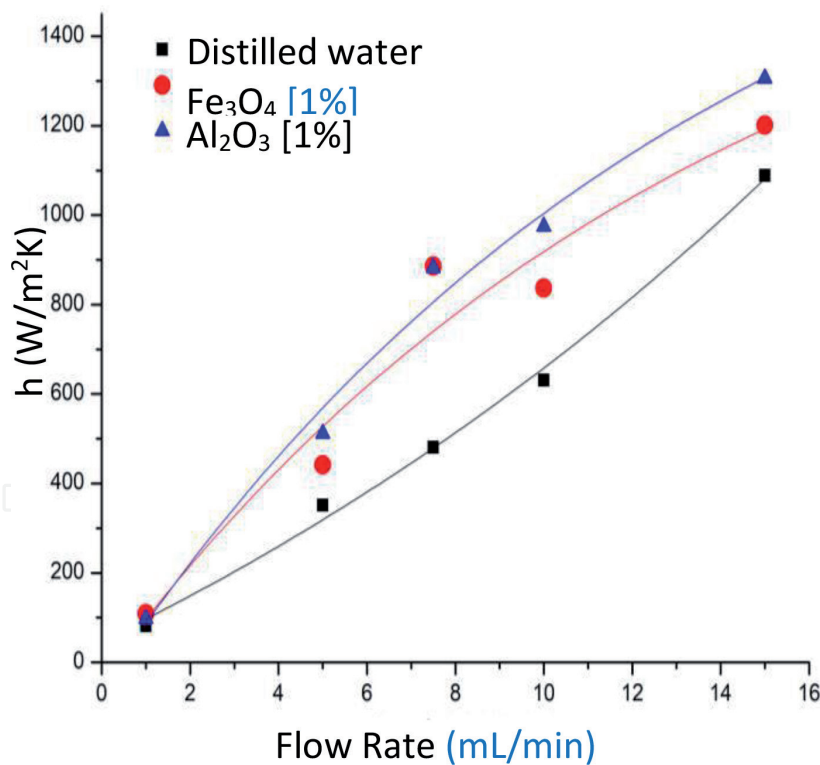

Figure 7.
Convective heat transfer coefficient of distilled water, alumina, and iron oxide nanofluids as the function of the flow rate.

Figure 9 compares the convective heat transfer coefficient for two different concentrations of NPs, i.e., 1 and 2.5% of both Fe_3O_4 and Al_2O_3. From a macroscopic view, it was noted a better dispersion for the nanofluids containing 1% of NPs. In addition, by increasing the concentration, the heat transfer was not enhanced. In fact, it was noted a decrease of the convective heat transfer coefficient when the concentration of NPs was increased to 2.5%. Although these results are somewhat
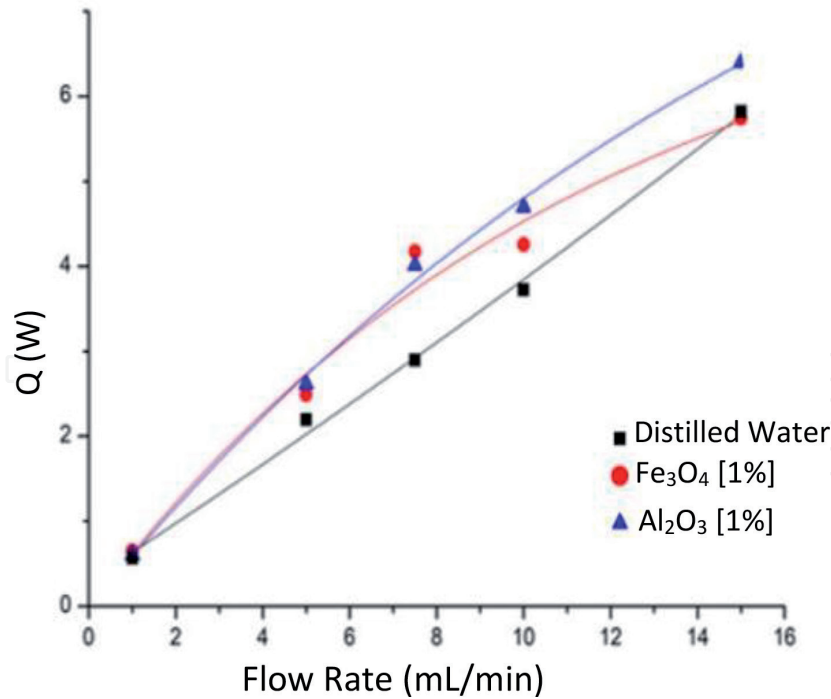
Figure 8.
Heat transfer rate of distilled water, alumina, and iron oxide nanofluids as the function of the flow rate.
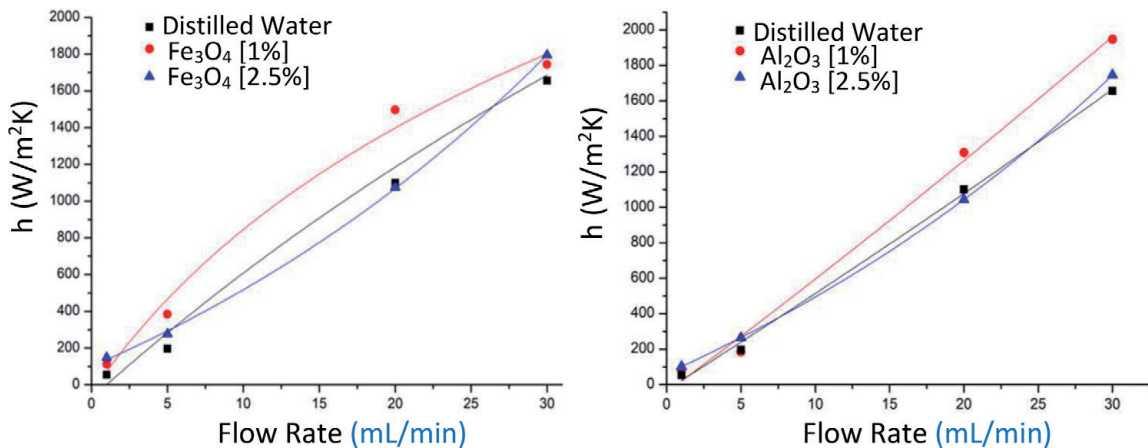

Figure 9.
Convective heat transfer coefficient of nanofluids as the function of the flow rate, for two different concentrations of alumina and iron oxide NPs.

paradoxical, other researchers, such as Wen and Ding [45] and Putra et al. [46], have reported similar results. The main possible reasons for the seen heat transfer deterioration include both the aggregation and sedimentation of the NPs. However, the possible reasons and mechanism attributed to such phenomena require further research. Currently, our group is carrying out both experimental and numerical work to identify the exact causes for such phenomena.

3.2 Optical and thermal imaging analyses

The biggest advantage of the developed PDMS heat sink device is the ability to visualize the flow phenomena happening inside the microchannels. By using a high-speed video microscopy system, it was possible to visualize several flow phenomena of the nanofluids such as the formation, growing, and breakdown of NPs clusters (see **Figure 10**). From these observations, it was concluded that one of the main causes for the formation of the clusters was the high roughness of the PDMS surface
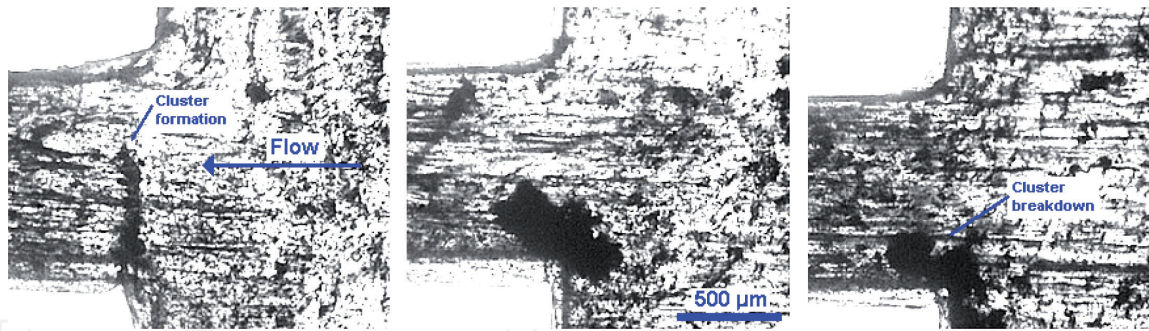
Figure 10.
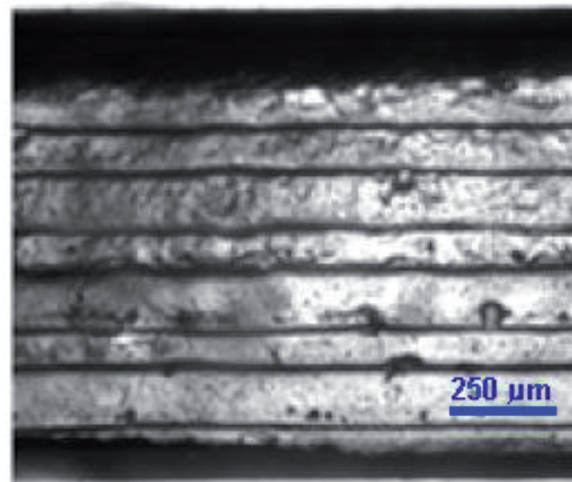*Optical images of the formation, growing, and breakdown of a cluster of NPs.*

Figure 11.
Optical image of the surface roughness of the heat sink device used in this study.

channels (**Figure 11**). This verified roughness was caused by the ABS master mold fabricated by the FDM 3D printer. In order to improve the surface roughness, the ABS master molds should undergo an acetone vapor treatment before performing the PDMS casting procedure. More detailed information about this method can be found elsewhere [27].

Another interesting advantage of this PDMS microfluidic device is the ability to visualize both the flow and thermal performance of the system by using a thermographic camera, as shown in **Figure 12**. Notice that the temperatures acquired were from the surface of the heat sink device and not directly from the working fluid flowing in the microchannels. In fact, PDMS is transparent to visible radiation but partially opaque to the infrared (IR) radiation. Hence, to obtain the temperatures more closely related to the working fluids flowing through the microchannels, the thickness of the upper walls should be reduced in future experiments. A very interesting observation was the ability to detect bubbles that are likely to happen in microfluidic devices. In **Figure 13**, it is possible to visualize a bubble within the microchannel and the thermal performance of the heat sink device.

3.3 Limitations and future directions

In this study, a microchannel device was successfully manufactured and used in microfluidic essays. Nevertheless, some limitations arose throughout the work. Despite the advantages of using PDMS, some properties of the material, such as
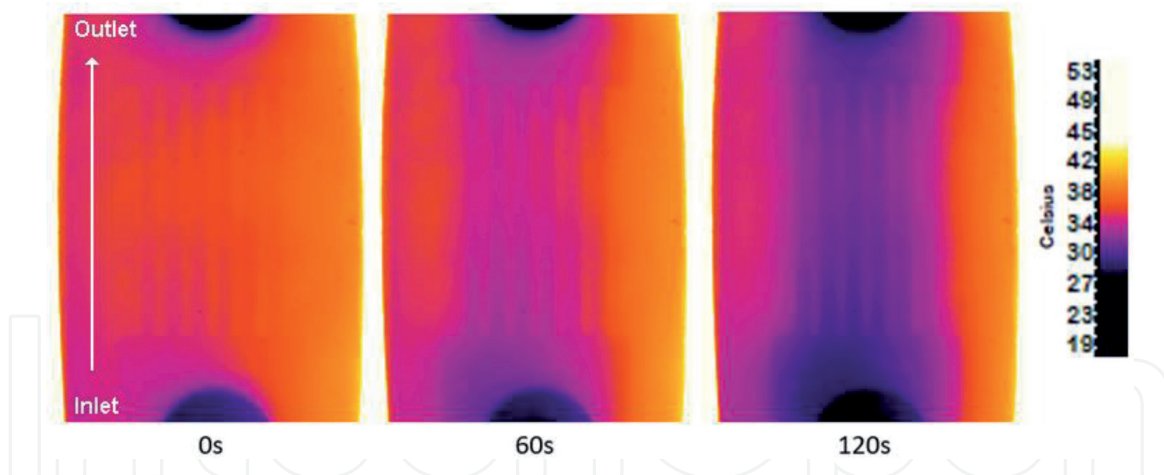
Figure 12.
Temperature gradient analyzed through the thermographic camera at three different instants: t = 0 s; t = 60 s, and t = 120 s.
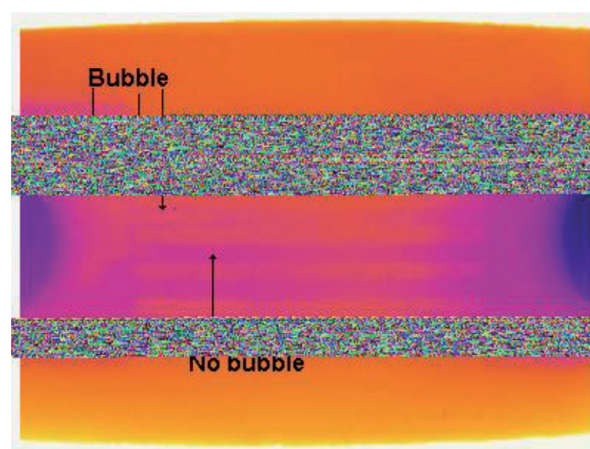

Figure 13.
Formation of a bubble at the entrance of the microchannels, which affects the thermal performance of the microfluidic device.

the low conductivity and partial opacity to the infrared (IR) radiation, were not favorable for the experiments. Also, the walls of the heat sink were rough due to the ABS master mold used in the fabrication technique, and the thickness should be reduced. The stability of the nanofluids has yet to be optimized since the deposition of NPs was detected on the heat sink walls. Future works will aim to improve of those limitations.

4. Conclusion

The main objective of this work was to show the potential of a PDMS heat sink microfluidic device to perform flows and heat transfer studies of nanofluids. The PDMS heat sink device was produced by using the FDM 3D printing process, combined with a PDMS casting technique. This fabrication process allowed to manufacture devices in an easy, low-cost, and reasonable reproductively way. To demonstrate the potential of the produced PDMS heat sink device, fluid flow and heat transfer studies were performed by using two different nanofluids, i.e., alumina (Al_2O_3)- and iron oxide (Fe_3O_4)-based nanofluids with concentrations of 1 and 2.5%. Overall, it was found that the thermal performance of the working nanofluids

is in good agreement with several past studies. For instance, it was noted that the heat energy absorbed by both nanofluids was higher than that absorbed by the distilled water. In addition, it was found that the flow rate affects the amount of heat absorbed by the nanofluids. However, the most interesting and unique results were the optical and thermal imaging results. These results were only possible due to the optical transparency of the PDMS heat sink device. Hence, by using this device, it was possible to visualize several flow phenomena of the nanofluids such as the formation, growing, and breakdown of NPs clusters. From these latter observations, it was possible to conclude that one of the main causes for the formation of the clusters was the high roughness of the PDMS surface channels caused by the surface roughness of the ABS master mold fabricated by the FDM 3D printer. This drawback can be overcome by performing an acetone vapor treatment before performing the PDMS casting. Overall, the simplicity, low-cost, and unique features of the proposed PDMS heat sink microfluidic device may prove a viable alternative tool to investigate nanofluids flow and heat transfer phenomena that are not possible to be performed by the current traditional systems.

Acknowledgements

Conflict of interest

The authors declare no conflict of interest.

Nomenclature

A	area
cp	heat capacity
h	convection heat transfer coefficient
K	thermal conductivity
N	number of microchannels
q	volume flow rate
Q	heat rate
R	resistance
Rt	thermic resistance
T	temperature
wp	average width of fin
zc	height of the channel

Greek symbols

η	fin efficiency
μ	viscosity
φ	nanoparticle concentration
ρ	density

Subscript

b	microchannel bottom
bf	base fluid
ext.	exterior
f	fluid
in	inlet
l	microchannel sidewall
nf	nanofluid
out	outlet
p	nanoparticles

Author details

Inês Maia[1], Cesar Rocha[2], Pedro Pontes[1], Vanessa Cardoso[3], João M. Miranda[4], Ana S. Moita[1], G. Minas[3], António L.N. Moreira[1] and Rui Lima[2,4*]

1 IN+ Center for Innovation, Technology and Policy Research, Instituto Superior Técnico, Universidade de Lisboa, Lisboa, Portugal

2 MEtRICs, Mechanical Engineering Department, University of Minho, Guimarães, Portugal

3 CMEMS-UMinho, University of Minho, Guimarães, Portugal

4 CEFT, Faculdade de Engenharia da Universidade do Porto (FEUP), Porto, Portugal

*Address all correspondence to: rl@dem.uminho.pt

13

References

[1] Moura M, Teodori E, Moita AS, Moreira ALN. 2 phase microprocessor cooling system with controlled pool boiling of dielectrics over micro- and-nano structured integrated heat spreaders. In: 15th IEEE Intersociety Conference on Thermal and Thermomechanical Phenomena in Electronic Systems (ITherm). 2016. pp. 378-387

[2] Abreu VTB e. Test and optimization of a two-phase thermosyphon cooling system for microprocessors under real working conditions. Instituto Superior Técnico; 2017

[3] Abreu V, Harrison M, Gess J, Moita AS. Two-phase thermosiphon cooling using integrated heat spreaders with copper microstructures. In: Proc 17th Intersoc Conf Therm Thermomechanical Phenom Electron Syst ITherm 2018. 2018. pp. 645-652

[4] Lameiras MM. Development of a Custom Made Condenser for a Two-Phase Thermosyphon CPU Cooling System. Instituto Superior Técnico; 2018

[5] Cahill DG, Braun PV, Chen G, Clarke DR, Fan S, Goodson KE, et al. Nanoscale thermal transport. II. 2003-2012. Applied Physics Reviews. 2014;**1**(1):11305-5-11305-6. Available from: http://aip.scitation.org/doi/10.1063/1.4832615

[6] Lomascolo M, Colangelo G, Milanese M, De Risi A. Review of heat transfer in nanofluids: Conductive, convective and radiative experimental results. Renewable and Sustainable Energy Reviews. 2015;**43**:1182-1198. DOI: 10.1016/j.rser.2014.11.086

[7] Godson L, Raja B, Mohan Lal D, Wongwises S. Enhancement of heat transfer using nanofluids—An overview. Renewable and Sustainable Energy Reviews. 2010;**14**(2):629-641

[8] Saidur R, Leong KY, Mohammad HA. A review on applications and challenges of nanofluids. Renewable and Sustainable Energy Reviews. 2011;**15**(3):1646-1668. DOI: 10.1016/j.rser.2010.11.035

[9] Philip J, Shima PD. Thermal properties of nanofluids. Advances in Colloid and Interface Science. 2012;**183-184**:30-45

[10] Ma DD, Xia GD, Wang J, Yang YC, Jia YT, Zong LX. An experimental study on hydrothermal performance of microchannel heat sinks with 4-ports and offset zigzag channels. Energy Conversion and Management. 2017;**152**:157-165

[11] Xuan Y, Roetzel W. Conceptions for heat transfer correlation of nanofluids. International Journal of Heat and Mass Transfer. 2000;**43**(19):3701-3707

[12] Philip J, Shima PD, Raj B. Evidence for enhanced thermal conduction through percolating structures in nanofluids. Nanotechnology [Internet]. 30 Jul 2008;**19**(30):305706 (7pp). Available from: http://stacks.iop.org/0957-4484/19/i=30/a=305706?key=crossref.3d918427472835fc73f454942400dcac

[13] Zhu H, Zhang C, Liu S, Tang Y, Yin Y. Effects of nanoparticle clustering and alignment on thermal conductivities of Fe_3O_4 aqueous nanofluids. Applied Physics Letters. 2006;**89**(2):4-7

[14] Pang C, Lee JW, Kang YT. Review on combined heat and mass transfer characteristics in nanofluids. International Journal of Thermal Sciences. 2015;**87**:49-67. DOI: 10.1016/j.ijthermalsci.2014.07.017

[15] Abareshi M, Goharshadi EK, Mojtaba Zebarjad S, Khandan Fadafan H, Youssefi A. Fabrication, characterization

and measurement of thermal conductivity of Fe$_3$O$_4$ nanofluids. Journal of Magnetism and Magnetic Materials. 2010;**322**(24):3895-3901. DOI: 10.1016/j.jmmm.2010.08.016

[16] Xia GD, Liu R, Wang J, Du M. The characteristics of convective heat transfer in microchannel heat sinks using Al$_2$O$_3$ and TiO$_2$ nanofluids. International Communications in Heat and Mass Transfer. 2016;**76**:256-264

[17] Gavili A, Zabihi F, Isfahani TD, Sabbaghzadeh J. The thermal conductivity of water base ferrofluids under magnetic field. Experimental Thermal and Fluid Science. 2012;**41**:94-98. DOI: 10.1016/j.expthermflusci.2012.03.016

[18] Kim S, Tserengombo B, Choi SH, Noh J, Huh S, Choi B, et al. Experimental investigation of heat transfer coefficient with Al$_2$O$_3$ nanofluid in small diameter tubes. Applied Thermal Engineering. 2019;**146**:346-355. DOI: 10.1016/j.applthermaleng.2018.10.001

[19] Al-Rjoub MF, Roy AK, Ganguli S, Banerjee RK. Enhanced heat transfer in a micro-scale heat exchanger using nano-particle laden electro-osmotic flow. International Communications in Heat and Mass Transfer. 2015;**68**:228-235. DOI: 10.1016/j.icheatmasstransfer.2015.09.009

[20] Al-Rjoub MF, Roy AK, Ganguli S, Banerjee RK. Enhanced electro-osmotic flow pump for micro-scale heat exchangers. In: ASME 2012 Third International Conference on Micro/Nanoscale Heat and Mass Transfer [Internet]. American Society of Mechanical Engineers; 2012. pp. 829-833. Available from: https://asmedigitalcollection.asme.org/MNHT/proceedings/MNHMT2012/54778/829/269200

[21] Faustino V, Catarino SO, Lima R, Minas G. Biomedical microfluidic devices by using low-cost fabrication techniques: A review. Journal of Biomechanics. 2016;**49**(11):2280-2292

[22] Catarino SO, Rodrigues RO, Pinho D, Minas G, Lima R. Blood cells separation and sorting techniques of passive microfluidic devices: From fabrication to applications. Micromachines. 2019;**10**:593. DOI: 10.3390/mi10090593

[23] Schneider F, Fellner T, Wilde J, Wallrabe U. Mechanical properties of silicones for MEMS. Journal of Micromechanics and Microengineering. 2008;**18**(6):065008 (9pp)

[24] Moreira NRP. Estudo de várias propriedades mecânicas do polidimetilsiloxano (PDMS) usado em dispositivos biomédicos. Instituto Politécnico de Bragança; 2013

[25] Saggiomo V, Velders AH. Simple 3D printed scaffold-removal method for the fabrication of intricate microfluidic devices. Advancement of Science. 2015;**2**(9):1500125

[26] Khanafer K, Duprey A, Schlicht M, Berguer R. Effects of strain rate, mixing ratio, and stress-strain definition on the mechanical behavior of the polydimethylsiloxane (PDMS) material as related to its biological applications. Biomedical Microdevices. 2009;**11**(2):503-508

[27] Pinho D, Bento D, Ribeiro J, Lima R, Vaz M. An In vitro experimental evaluation of the displacement field in an intracranial aneurysm model. In: Flores P, Viadero F, editors. New Trends in Mechanism and Machine Science. Cham: Springer International Publishing; 2015. pp. 261-268

[28] Mata A, Fleischman AJ, Roy S. Characterization of polydimethylsiloxane (PDMS) properties for biomedical micro/nanosystems. Biomedical Microdevices. 2005;**7**(4):281-293

[29] Ainla A. Valves for microfluidic devices [Internet]. Chalmers University of Technology; 2007. Available from: http://www.ims.ut.ee/~alar/microtech/Ch1_4/Ch_1_4_4.php

[30] Comina G, Suska A, Filippini D. 3D printed unibody lab-on-a-chip: Features survey and check-valves integration. Micromachines. 2015;**6**(4):437-451

[31] Gaal G, Mendes M, de Almeida TP, Piazzetta MHO, Gobbi ÂL, Riul A, et al. Simplified fabrication of integrated microfluidic devices using fused deposition modeling 3D printing. Sensors and Actuators B: Chemical. 2017;**242**:35-40. DOI: 10.1016/j.snb.2016.10.110

[32] Faria CL, Pinho D, Santos J, Gonçalves LM, Lima R. Low cost 3D printed biomodels for biofluid mechanics applications. Journal of Mechanical Engineering and Biomechanics. 2018;**3**(1):1-7

[33] Yap YL, Tan YSE, Tan HKJ, Peh ZK, Low XY, Yeong WY, et al. 3D printed bio-models for medical applications. Rapid Prototyping Journal. 2017;**23**(2):227-235

[34] Souza A, Ribeiro J, Lima R. Manufacturing process of a brain aneurysm biomodel in PDMS using rapid prototyping. In: Lecture Notes in Computational Vision and Biomechanics. Berlin: Springer Nature; 2019

[35] Cardoso VF, Irusta S, Navascues N, Lanceros-Mendez S. Comparative study of sol-gel methods for the facile synthesis of tailored magnetic silica spheres. Materials Research Express. 2016;**3**(7):1-7. DOI: 10.1088/2053-1591/3/7/075402

[36] Lima R, Vega EJ, Cardoso VF, Minas G, Montanero JM. Magnetic PDMS microparticles for biomedical and energy applications. In: Lecture Notes in Computational Vision and Biomechanics. Berlin: Springer Nature; 2019

[37] Cardoso VF, Miranda D, Botelho G, Minas G, Lanceros-Méndez S. Highly effective clean-up of magnetic nanoparticles using microfluidic technology. Sensors and Actuators B: Chemical. 2018;**255**:2384-2391. DOI: 10.1016/j.snb.2017.08.095

[38] Teodori E, Pontes P, Moita AS, Moreira ALN. Thermographic analysis of interfacial heat transfer mechanisms on droplet/wall interactions with high temporal and spatial resolution. Experimental Thermal and Fluid Science. 2018;**96**:284-294. DOI: 10.1016/j.expthermflusci.2018.03.013

[39] Lamas B, Abreu B, Fonseca A, Martins N, Oliveira M. Critical analysis of the thermal conductivity models for CNT based nanofluids. International Journal of Thermal Sciences. 2014;**78**:65-76. DOI: 10.1016/j.ijthermalsci.2013.11.017

[40] Aybar H, Sharifpur M, Azizian MR, Mehrabi M, Meyer JP. A review of thermal conductivity models for nanofluids. Heat Transfer Engineering. 2015;**36**(13):1085-1110

[41] Pak BC, Cho YI. Hydrodynamic and heat transfer study of dispersed fluids with submicron metallic oxide particles. Experimental Heat Transfer. 1998;**11**(2):151-170

[42] Pavlik M. The dependence of suspension viscosity on particle size, shear rate, and solvent viscosity. 2009. Available from: http://via.library.depaul.edu/etd/71

[43] Chein R, Chuang J. Experimental microchannel heat sink performance studies using nanofluids. International Journal of Thermal Sciences. 2007;**46**(1):57-66

[44] Wen D, Ding Y. Experimental investigation into convective heat transfer of nanofluids at the entrance region under laminar flow conditions.

International Journal of Heat and Mass
Transfer. 2004;**47**(24):5181-5188

[45] Wen D, Ding Y. Formulation of
nanofluids for natural convective heat
transfer applications. International
Journal of Heat and Fluid Flow.
2005;**26**(6):855-864

[46] Putra N, Roetzel W, Das SK. Natural
convection of nano-fluids. Heat and
Mass Transfer. 2003;**39**(8-9):775-784